

CREEP OF A CAST INTERMETALLIC TiAl-BASED ALLOY

JURAJ LAPIN

*Institute of Materials and Machine Mechanics, Slovak Academy of Sciences,
Račianska 75, 831 02 Bratislava, Slovak Republic*

Received 12 October 2004, accepted 25 October 2004

Creep of a cast intermetallic TiAl-based alloy with the chemical composition Ti-46.88Al-1.96W-0.53Si (at.%) was studied in the temperature range from 700 to 800 °C and at tensile stresses ranging from 200 to 390 MPa. Analysis of the creep data in the terms of the threshold stress concept and using the stress normalized with respect to the temperature dependence of the shear modulus gives true activation energy for creep of $Q = 365 \pm 17$ kJ/mol and stress exponent of $n = 5$. This value is close to the activation energy for lattice diffusion of Al in TiAl. Transmission electron microscopy (TEM) investigations revealed that the deformation microstructures are dominated by ordinary dislocations in the γ -matrix. Dislocations are elongated in the screw orientation and frequently pinned along their lengths. Kinetics of the creep deformation within the studied temperature range and applied stresses is controlled by non-conservative motion of ordinary dislocations.

Key words: intermetallics, titanium aluminides, TiAl, creep, deformation microstructure

1. Introduction

Continual effort to improve energy efficiency and to reduce polluting emissions in transport and energy generation sectors can be partly achieved by reducing the weight of engineering components. In recent years there is particular interest in emerging class of ordered TiAl-based intermetallic alloys for various high-temperature structural applications in the gas turbine industry including turbine blades in the last stage of the low-pressure turbine, high-pressure compressor blades, vanes, and casings [1, 2]. In the automotive industry, the potential applications are mainly automotive exhaust valves and turbocharger wheels [3].

As was shown in our recent studies [4–7], the microstructure of large investment cast turbine blades after post-solidification thermo-mechanical treatment combined

e-mail: ummslapi@savba.sk

with subsequent heat treatments is not homogeneous and changes from fully or nearly lamellar in the vicinity of the blade surface to duplex one in the central part. Such microstructural changes affect significantly local mechanical properties of the blades. Although many studies were published on the creep of various TiAl-based alloys, information about creep of large cast components like turbine blades are still lacking in the literature. Therefore, evaluation of creep behaviour of samples prepared from such large components is of great practical interest.

The aim of this paper is to study creep of TiAl-based alloy prepared by casting in the form of a large gas turbine blade. The analysis of the experimental data is based on the threshold stress concept recently widely used by Čadek and co-workers [8–13] and aims at reconciling the creep characteristics including the stress exponent and activation energy for creep to those measured for self-diffusion in single phase TiAl-based alloys.

2. Experimental procedure

Creep experiments were conducted on the alloy with the chemical composition Ti-46.88Al-1.96W-0.53Si (at.%). The material was provided by Alstom Ltd. in the form of an investment cast turbine blade. The alloy was developed by Nazmy and Staubli [14] for investment cast turbine blades and turbocharger wheels with improved creep properties. The as-received material was subjected to a hot isostatic pressing at an applied pressure of 172 MPa and a temperature of 1260°C for 4 h, which was followed by solution annealing at 1350°C for 1 h and gas fan cooling. The heat treatment was completed by stabilization annealing at 1000°C for 6 h and furnace cooling to room temperature.

Tensile creep specimens with a gauge length of 20 mm and gauge diameter of 4 mm were cut from the central part of the cast blade by electro-spark machining. After lath machining, the specimen surface was polished to a roughness of about 0.3 μm . Constant load creep tests were performed at temperatures of 700, 750, and 800°C under initial tensile stresses ranging from 200 to 390 MPa. The specimen displacement was measured using a high-temperature extensometer attached to the ledges of the creep specimen. The extensometer was equipped with a linear variable displacement transformer (LVDT). The acquisition of time-elongation data was accomplished by a computer and data processing was performed by a computer program. Note, that the creep strain was only several percent (up to 3 %). Therefore, obtained results can be considered to correspond also to results of the tests under constant stress.

Microstructural analysis was performed by optical microscopy (OM), scanning electron microscopy (SEM), transmission electron microscopy (TEM), and energy dispersive X-ray (EDX) spectroscopy. OM and SEM samples were prepared using standard metallographic techniques and etched in a reagent of 150 ml H₂O, 25 ml HNO₃, and 10 ml HF. TEM samples were thinned mechanically to a thickness of

about 40 μm and then by ion milling until perforation. Volume fraction and size of coexisting phases were determined by computerized image analysis.

3. Results

3.1 Microstructure before creep

Fig. 1 shows the typical microstructure of the alloy before creep. The equiaxed grains with an average grain size of about 600 μm have a pseudo-duplex (PD) microstructure. The microstructure within the grains consists of lamellar (66 vol.%), feathery (26 vol.%), and γ -rich (8 vol.%) regions. The lamellar regions contain discontinuous lamellae in the γ -matrix (ordered TiAl phase with $L1_0$ crystal structure). The discontinuous lamellae are composed of α_2 segments (ordered Ti_3Al phase with $D0_{19}$ crystal structure), fine needle-like B2 particles, and Ti_5Si_3 precipitates, as seen in Fig. 2 [6]. The feathery regions are composed of the γ -phase, irregular, partially decomposed α_2 lamellae, B2 particles, and Ti_5Si_3 precipitates. The γ -rich region is composed of the γ -matrix and spherical Ti_5Si_3 precipitates. A major difference between pseudo-duplex and duplex type of microstructure is that the γ -phase in the pseudo-duplex structure is crystallographically identical to

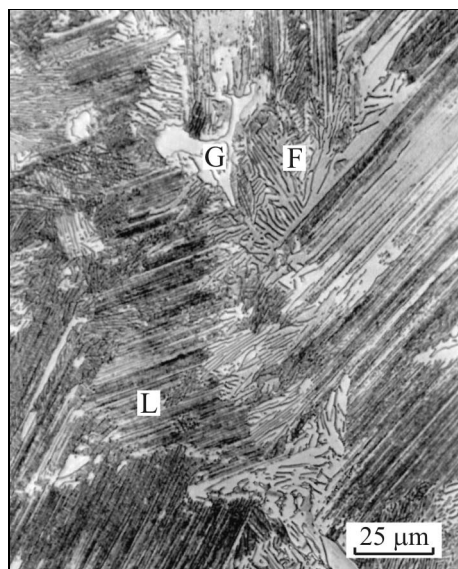


Fig. 1. Light micrograph showing the typical microstructure of the specimens before creep: L – lamellar microstructure, F – feathery microstructure, G – γ -rich region.

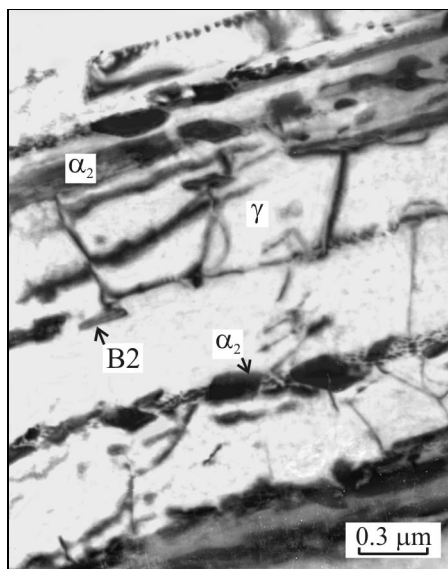


Fig. 2. TEM micrograph showing lamellar region with discontinuous α_2 lamellae before creep testing.

the neighbouring γ -phase in the lamellar colonies [15]. It should be noted that the alloy exhibited very low dislocation density in all regions before creep testing, as seen in Fig. 2.

3.2 Creep

For rotating components like turbine blades, the maximum overall creep strain depends on the engine tolerance and is usually less than 1 % [16]. From this point of view, the primary and adequate part of secondary creep stage is of the largest interest. Fig. 3 shows the variation of the instantaneous creep rate with the strain at a temperature of 800 °C. During the primary creep stage the creep rate decreases with increasing strain. After reaching its minimum at a strain of about 1 %, the creep rate continuously increases with increasing strain. The minimum creep rates $\dot{\epsilon}_{\min}$ and the applied stresses σ were fitted to the power law

$$\dot{\epsilon}_{\min} = A\sigma^n, \quad (1)$$

where A is a constant and n is the stress exponent. Fig. 4 shows variation of the minimum creep rate with the applied stress. Using linear regression analysis of the creep data, the stress exponent is determined to vary from 7.3 to 7.6. The correlation coefficients r^2 of these fits are better than 0.96. The measured stress

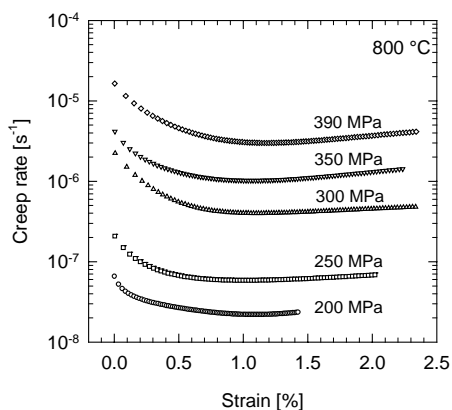


Fig. 3. Variation of the instantaneous creep rate with the strain at 800 °C. The applied stresses are indicated in the figure.

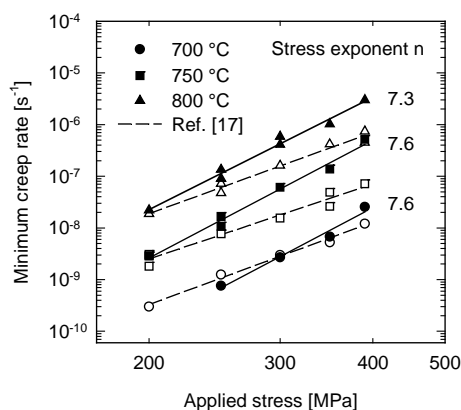


Fig. 4. Dependence of the minimum creep rate on the applied stress. The open and closed symbols belong to the data reported in Ref. [17] and data measured in the present work, respectively. Testing temperatures and calculated stress exponents n are indicated in the figure.

exponents are higher than those ranging from 4.8 to 5.3 reported for boron doped counterpart alloy with the chemical composition Ti-45.2Al-2W-0.6Si-0.7B (at.%) [17].

The stress-minimum creep rate-temperature data were also fitted to the Bailey-Norton power law expression

$$\dot{\epsilon}_{\min} = A' \sigma^n \exp\left(-\frac{Q_a}{RT}\right), \quad (2)$$

where A' is a constant, Q_a is the apparent activation energy for creep, R is the universal gas constant, and T is the absolute temperature. The apparent activation energy for creep Q_a is calculated according to equation in the form

$$Q_a = \left[\frac{\partial \ln \dot{\epsilon}_{\min}}{\partial (1/RT)} \right]_{\sigma=\text{const}}. \quad (3)$$

The apparent activation energy calculated for five different applied stresses at three different temperatures is 421 ± 16 kJ/mol. This value is higher than that of 250–295 kJ/mol and 358 kJ/mol determined for self-diffusion of Ti and Al in TiAl, respectively [18].

3.3 Microstructure after creep

Deformation in two-phase TiAl-based alloys is well known to occur by ordinary dislocations with a Burgers vector $b = 1/2\langle 110 \rangle$ and to a lesser extent by mechanical twinning along $1/6\langle 112 \rangle$ and $\{111\}$ and by superdislocations with the Burgers vector $\langle 110 \rangle$ and $1/2\langle 112 \rangle$ [19]. Microstructural observations revealed that the creep of the studied alloy at creep strain of about 1.5 % is dominated by $1/2\langle 110 \rangle$ type of ordinary dislocations. Fig. 5 shows the typical deformation microstructure of the specimen in the lamellar region where the α_2 lamellae are decomposed to the γ -phase and needle-like B2 precipitates. The dislocations in the γ -matrix tend

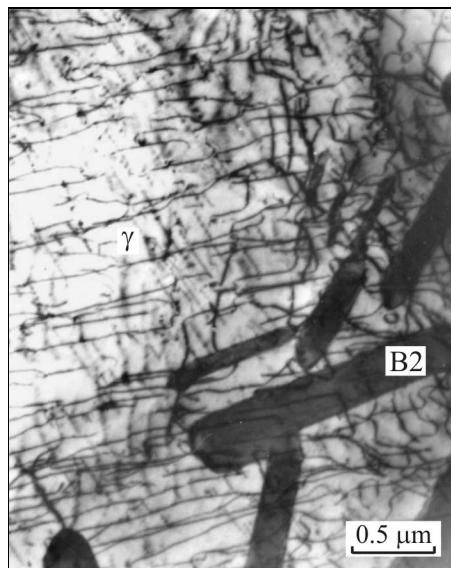


Fig. 5. TEM micrograph showing the deformation microstructure in the vicinity of needle-like B2 precipitates after 1.5 % creep strain at 750°C and 200 MPa.

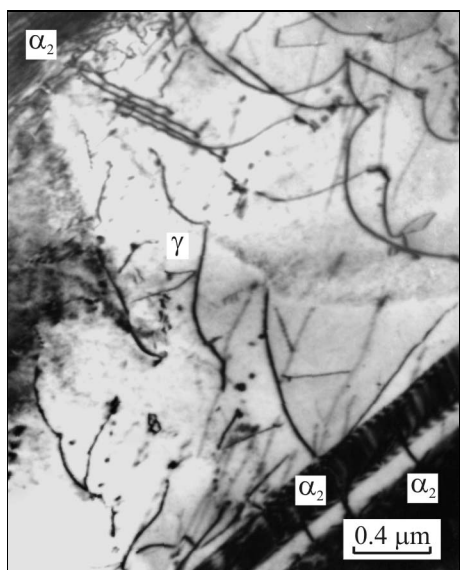


Fig. 6. TEM micrograph showing the deformation microstructure of the lamellar region after 1.5 % creep strain. Creep test at 750°C and 200 MPa.

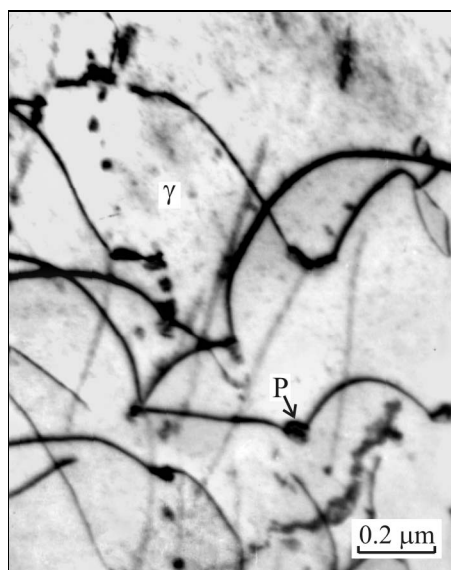


Fig. 7. TEM micrograph showing interactions of dislocations with fine precipitates after 1.5 % creep strain at 750°C and 200 MPa. P – Ti_5Si_3 precipitate.

to be elongated in the screw orientation and appear to be frequently pinned along their lengths. The dislocation segments form local cusps along the length of the dislocations. Such cusps are frequently associated with the tall jogs on the screw segments of dislocations [20]. The dislocation segments bowing between the jogs lie on parallel $\{111\}$ planes, and the jogs themselves lie on a cross slip plane [21]. Using in-situ TEM experiments, Appel showed [22] that the jogs move by climbing under the combined action of thermomechanical stresses and osmotic climb forces arising from the chemical potential of the excess of vacancies. Depending on the crystallographic orientation of needle like B2 precipitates in the γ -matrix, some precipitates are easily passed by dislocations generated in the matrix. However, there are many B2 precipitates, which are effective obstacles to dislocation motion. The dislocations overcome these precipitates by Orowan bowing mechanism leaving dislocation loops around them, as seen in Fig. 5. Fig. 6 shows the typical deformation microstructure in the lamellar region with remaining α_2 lamellae. The deformation is inhomogeneous with smaller dislocation densities in the thinner γ lamellae and significantly larger densities in the thicker γ lamellae. Lamellar γ/α_2 interfaces appear to constrain effectively deformation to individual γ -lamellae with little evidence for direct transmission of dislocations under applied creep condi-

tions. The thicker lamellae have ordinary dislocations that are often cusped in configuration similar to that shown in Fig. 5. The stress necessary to move these channelling dislocations must overcome bowing stress [23]. Fig. 7 shows strong interactions of ordinary dislocations with fine Ti_5Si_3 precipitates. Apparently, the dislocations are pinned at the departure part of the precipitates. The deformation microstructure in the γ -rich region is also characterized by pinned ordinary dislocations and by formation of prismatic dislocation loops similar to that shown in Fig. 5. Coarse Ti_5Si_3 particles are observed to be effective obstacles to dislocation motion, and intensive pile-up at γ -matrix/ Ti_5Si_3 interfaces was observed. Seo et al. [24] suggested for Ti-48Al-2W (at.%) alloy that solute tungsten hinders dislocation glide within the γ -matrix increasing the relative importance of non-conservative motion of dislocations and vacancy assisted mechanisms.

4. Discussion

The stress exponent measured in this work is higher than the values n of about 3 or 5 commonly observed in pure metals and single-phase alloys for the creep controlled by dislocation glide or climb, respectively [25]. In TiAl-based alloys, high values of the stress exponent and activation energy for creep have been justified by considering the existence of friction [26] or threshold stress [27] resulting from inhomogeneous deformation or hindering dislocation motion by particles, respectively. The applied stress is then reduced by the amount of such stresses. We can examine if the same approach could reconcile the values of n and Q_a measured for the studied alloy with physically sound values of n and activation energy for self-diffusion in the TiAl matrix. In the following analysis, we will assume that the creep of the alloy is governed by a driving stress $\sigma_d = \sigma - \sigma_{th}$, where σ_{th} is the threshold stress [8–13].

The stress reduction test has been widely used to identify the controlling mechanisms or to measure internal stresses in creep of metallic material [25, 28–32]. The presence or absence of an incubation period of zero creep in a stress reduction test can assist in determining whether mechanisms based on dislocation recovery (incubation period) or glide (no incubation period) control the creep of the alloy. Figs. 8a and 8b show the creep responses of the alloy during stress reduction (a) from 350 to 250 MPa at 750 °C and (b) from 250 to 200 MPa at 800 °C, respectively. In both cases, it can be clearly seen that creep begins after an incubation period of 5.3 and 1.7 h for the stress reduction experiments at 750 and 800 °C, respectively. Microstructural observations and stress reduction experiments suggest that the creep over the studied temperatures and applied stresses is controlled by non-conservative motion of dislocations characterized by a stress exponent of $n = 5$ measured in previous studies on TiAl-based alloys [17, 33]. Fig. 9 shows minimum creep rate normalized with respect to the stress exponent of 5 as a function of the applied stress. The extrapolations to zero creep rate at all creep temperatures

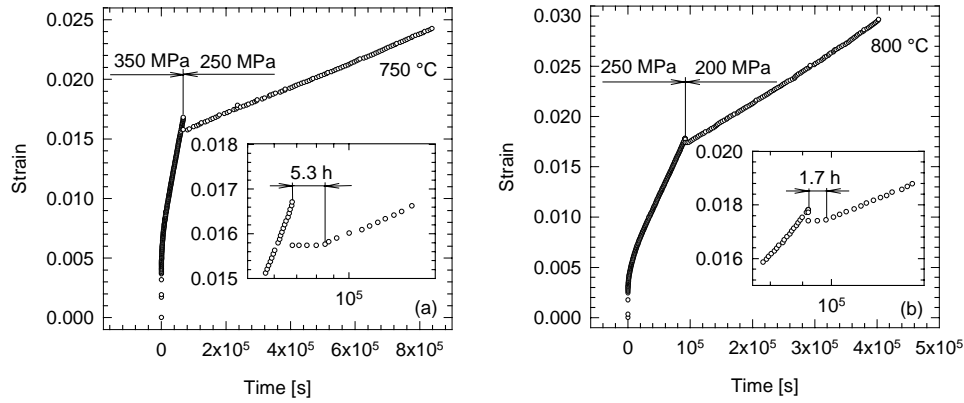


Fig. 8. Creep strain response during stress reduction tests: (a) from 350 to 250 MPa at 750 °C and (b) from 250 to 200 MPa at 800 °C. The incubation periods are apparent in the figures.

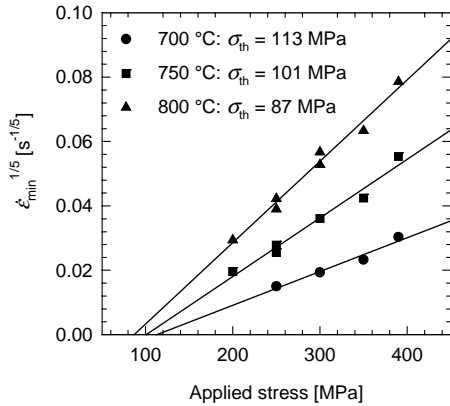


Fig. 9. Minimum creep rate normalized by the stress exponent of $n = 5$ as a function of the applied stress. The test temperatures and determined threshold stresses σ_{th} are given in the figure.

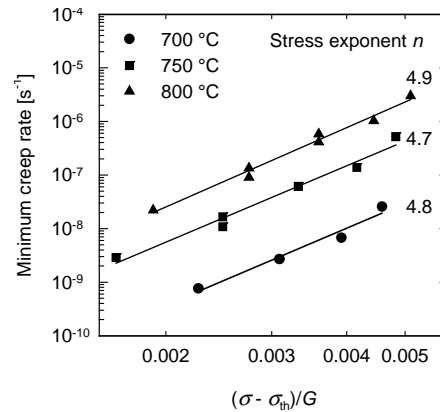


Fig. 10. Minimum creep rate as a function of the stress $(\sigma - \sigma_{th})$ normalized by the temperature dependence of the shear modulus G .

intersect the abscissa at values of $\sigma > 0$. This is not in agreement with Eqs. (1) and (2) and thus indicates the existence of threshold stress. It is clear from Fig. 9 that the values of threshold stresses are significantly high (113 MPa at 700 °C, 101 MPa at 750 °C, and 87 MPa at 800 °C), and their effect on the creep cannot be

neglected. Therefore, we will assume that no appreciable creep of the material can occur below a minimum threshold stress σ_{th} necessary for dislocation to bypass the α_2 -segments, B2- and Ti_5Si_3 -precipitates, and remaining lamellar interfaces. The calculated driving stress ($\sigma - \sigma_{\text{th}}$) can be fitted to a power-law equation in the form

$$\dot{\epsilon}_{\text{min}} = B \left(\frac{\sigma - \sigma_{\text{th}}}{G} \right)^n, \quad (4)$$

where B is a constant and G is the shear modulus of the γ -matrix at a given temperature. Fig. 10 shows the minimum creep rate as function of the effective stress normalized with the temperature dependence of the shear modulus. The temperature dependence of the shear modulus $G(T) = 72.165 - 0.012T$ is determined from experimentally measured temperature dependence of the elastic modulus for the investigated alloy [16], where $G(T)$ is given in GPa. As seen from this figure, applying the concept of the threshold stress results in the stress exponents n close to 5 over the studied temperature range. Hence, the kinetic equation for the minimum creep rate of the alloy can be written in the form [25]

$$\dot{\epsilon}_{\text{min}} = B' \left(\frac{\sigma - \sigma_{\text{th}}}{G} \right)^n \exp \left(-\frac{Q}{RT} \right), \quad (5)$$

where B' is a constant and Q is the true activation energy for creep. The true activation energy for creep calculated from the temperature dependence of the constant B in Eq. (4) is $Q = 365 \pm 17$ kJ/mol. This value is comparable with a true activation energy for creep of $Q = 343 \pm 16$ kJ/mol reported by Lapin [17] for Ti-45.2Al-2W-0.6Si-0.7B (at.%) alloy or that for self-diffusion of Al in TiAl of 358 kJ/mol [18]. However, it is still significantly higher than those of 250–295 kJ/mol reported for self-diffusion of Ti in TiAl [18].

The strong stress dependence of minimum creep rate on the stress ($\sigma - \sigma_{\text{th}}$) with the stress exponent of $n = 5$ and the activation energy for creep close to that for self-diffusion of Al in TiAl indicates that the creep of the studied alloy can be also described by a classical Dorn kinetic equation in the form [25]

$$\dot{\epsilon}_{\text{min}} = B'' \left(\frac{\sigma - \sigma_{\text{th}}}{G} \right)^n \frac{Gb}{kT} D_0 \exp \left(-\frac{Q_L}{RT} \right), \quad (6)$$

where B'' is a dimensionless constant, b is the length of the Burgers vector, k is Boltzmann's constant, D_0 is the pre-exponential factor for diffusion, and Q_L is the activation energy for self-diffusion. Fig. 11 shows the minimum creep rate in a normalized form as a function of the effective stress. The data are referred to the absolute temperature, temperature dependence of the shear modulus, length of the

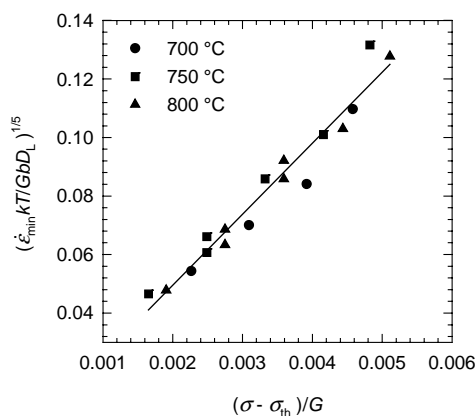


Fig. 11. Normalized minimum creep rate as a function of the normalized stress ($\sigma - \sigma_{th}$). The creep temperatures are indicated in the figure.

Burgers vector of $b = 0.28$ nm, and diffusion coefficient $D_L = D_0 \exp(-Q_L/RT)$, where $D_0 = 2.11 \times 10^{-2}$ m²/s, and the activation energy for self-diffusion of Al in TiAl is $Q_L = 358$ kJ/mol [18]. Linear regression analysis of the experimental data in Fig. 11 yields a kinetic equation for the minimum creep rate in the form

$$\dot{\epsilon}_{\min} = 8.9 \times 10^6 \left(\frac{\sigma - \sigma_{th}}{G} \right)^5 \frac{Gb}{kT} D_0 \exp\left(-\frac{358000}{RT}\right). \quad (7)$$

The correlation coefficient of this fit r^2 is 0.95.

It should be emphasized that the creep of the studied alloy is controlled by non-conservative motion of ordinary dislocations and no evidence for grain boundary sliding or sliding along lamellar interfaces accompanied by a decrease of the stress exponent at low stresses and creep rates reported for some TiAl-based alloys was observed [34, 35].

5. Conclusions

The investigation of creep behaviour of a cast intermetallic TiAl-based alloy with the chemical composition Ti-46.88Al-1.96W-0.53Si (at.%) yielded the following conclusions:

1. The minimum creep rate is found to depend strongly on the applied stress and temperature. Analysis of the creep data in the terms of the threshold stress concept and using the stress normalized with respect to the temperature dependence of the shear modulus gives true activation energy for creep of $Q = 365 \pm 17$ kJ/mol and stress exponent of $n = 5$.

2. TEM investigations reveal that the deformation microstructures in the lamellar, feathery, and γ -rich regions are dominated by $1/2\langle 110 \rangle$ type of ordinary

dislocations in the γ -matrix. The dislocations are elongated in the screw orientation and are frequently pinned along their lengths. The dislocation segments form local cusps along the length of the dislocations, which are frequently associated with the jogs on the screw segments of dislocations.

3. The stress reduction experiments, the true activation energy for creep, and deformation microstructures suggest that the kinetics of creep deformation over the experimental interval of temperatures and applied stresses is controlled by non-conservative motion of ordinary dislocations.

Acknowledgements

The author gratefully acknowledges the financial support of the Slovak Grant Agency for Science under the contract VEGA 2/4166/24. He also expresses his thanks to Dr. M. Nazmy from ALSTOM Ltd. for providing the experimental material.

REFERENCES

- [1] HARDING, R. A.: *Kovove Mater.*, 42, 2004, p. 225.
- [2] DIMIDUK, D. M.: *Mater. Sci. Eng. A*, 263, 1999, p. 281.
- [3] TETSUI, T.: *Mater. Sci. Eng. A*, 329–331, 2002, p. 582.
- [4] LAPIN, J.—NAZMY, M.: *Mater. Sci. Eng. A*, 380, 2004, p. 298.
- [5] LAPIN, J.—KLIMOVÁ, A.: *Kovove Mater.*, 41, 2003, p. 1.
- [6] LAPIN, J.—PELACHOVÁ, T.: *Kovove Mater.*, 42, 2004, p. 143.
- [7] LAPIN, J.—KLIMOVÁ, A.: *J. Mater. Sci. Lett.*, 22, 2003, p. 1275.
- [8] ČADEK, J.—KUCHAŘOVÁ, K.—ZHU, S.: *Kovove Mater.*, 39, 2001, p. 77.
- [9] ČADEK, J.—KUCHAŘOVÁ, K.—ZHU, S.: *Kovove Mater.*, 39, 2001, p. 221.
- [10] ČADEK, J.—KUCHAŘOVÁ, K.: *Kovove Mater.*, 40, 2002, p. 69.
- [11] ČADEK, J.—KUCHAŘOVÁ, K.: *Kovove Mater.*, 40, 2002, p. 133.
- [12] ČADEK, J.—KUCHAŘOVÁ, K.: *Kovove Mater.*, 41, 2003, p. 127.
- [13] ČADEK, J.—KUCHAŘOVÁ, K.: *Kovove Mater.*, 42, 2004, p. 9.
- [14] NAZMY, M.—STAUBLI, M.: U.S.Pat.#5,207,982 and European Pat.#45505 B1.
- [15] RECINA, V.—LUNDSTRÖM, D.—KARLSSON, B.: *Metall. Mater. Trans. A*, 33A, 2002, p. 2869.
- [16] NAZMY, M.—LUPINC, V.: In: *Materials for Advanced Power Engineering 2002*. Eds.: Lecomte-Beckers J., Carton M., Schubert F., Ennis P. J. Forschungszentrum Jülich GmbH, Vol. 21, Part I; 2002, p. 43.
- [17] LAPIN, J.: *Scripta Mater.*, 50, 2004, p. 261.
- [18] MISHIN, Y.—HERZIG, CH.: *Acta Mater.*, 48, 2000, p. 589.
- [19] APPEL, F.—WAGNER, R.: *Mater. Sci. Eng. R*, 22, 1998, p. 187.
- [20] KARTHIKEYAN, S.—VISWANATHAN, G. B.—GOUMA, P. I.—VASUDEVAN, V. K.—KIM, Y. W.—MILLS, M. J.: *Mater. Sci. Eng. A*, 329–331, 2002, p. 621.
- [21] KARTHIKEYAN, S.—VISWANATHAN, G. B.—MILLS, M. J.: *Acta Mater.*, 52, 2004, p. 2577.
- [22] APPEL, F.: *Intermetallics*, 9, 2001, p. 907.
- [23] NIX, W. D.: *Scripta Mater.*, 39, 1998, p. 545.
- [24] SEO, D. Y.—BEDDOES, J.—ZHAO, L.: *Metall. Mater. Trans. A*, 33A, 2003, p. 2177.
- [25] ČADEK, J.: *Creep in Metallic Materials*. New York, Elsevier Science Publishing Company, Inc. 1988.

-
- [26] ZHANG, W. J.—SPIGARELLI, S.—CERRI, E.—EVANGELISTA, E.—FRANCESCO-
CONI, L.: *Mater. Sci. Eng. A*, 211, 1996, p. 15.
- [27] GORZEL, A.—SAUTHOFF, G.: *Intermetallics*, 7, 1999, p. 371.
- [28] MILIČKA, K.—DOBEŠ, F.—SCHAFLER, E.—ZEHETBAUER, M.: *Kovove Ma-
ter.*, 41, 2003, p. 133.
- [29] MILIČKA, K.: *Kovove Mater.*, 37, 1999, p. 256.
- [30] MILIČKA, K.: *Kovove Mater.*, 37, 1999, p. 285.
- [31] MILIČKA, K.: *Kovove Mater.*, 37, 1999, p. 357.
- [32] MILIČKA, K.: *Acta Mater.*, 47, 1999, p. 1831.
- [33] PARTHASARATHY, T. A.—MENDIRATTA, M. G.—DIMIDUK, D. M.: *Scripta
Mater.*, 37, 1997, p. 315.
- [34] WANG, J. G.—NIEH, T. G.: *Intermetallics*, 8, 2000, p. 737.
- [35] WANG, J. N.—ZHU, J.—WU, J. S.—DU, X. W.: *Acta Mater.*, 50, 2002, p. 1307.